







## RESEARCH ARTICLE

# Disassembly of the apical junctional complex during the transmigration of *Leptospira interrogans* across polarized renal proximal tubule epithelial cells

Isabel Sebastián<sup>1</sup>  | Nobuhiko Okura<sup>2</sup> | Bruno M. Humbel<sup>3,4,5</sup> | Jun Xu<sup>6,1</sup>  |  
Idam Hermawan<sup>1</sup>  | Chiaki Matsuura<sup>1</sup>  | Malgorzata Hall<sup>3</sup> |  
Chitoshi Takayama<sup>2</sup> | Tetsu Yamashiro<sup>1</sup> | Shuichi Nakamura<sup>7</sup>  | Claudia Toma<sup>1</sup> 

<sup>1</sup>Department of Bacteriology, Graduate School of Medicine, University of the Ryukyus, Okinawa, Japan

<sup>2</sup>Department of Molecular Anatomy, Graduate School of Medicine, University of the Ryukyus, Okinawa, Japan

<sup>3</sup>Imaging Section, Okinawa Institute of Science and Technology Graduate University, Okinawa, Japan

<sup>4</sup>Microscopy Center, Universidade Federal de Minas Gerais, Belo Horizonte, Brazil

<sup>5</sup>Department of Cell Biology and Neuroscience, Juntendo University Graduate School of Medicine, Tokyo, Japan

<sup>6</sup>Department of Animal Microbiology, Graduate School of Agricultural Science, Tohoku University, Sendai, Japan

<sup>7</sup>Department of Applied Physics, Graduate School of Engineering, Tohoku University, Sendai, Japan

## Correspondence

Claudia Toma, Department of Bacteriology, Graduate School of Medicine, University of the Ryukyus, Okinawa 903-0215, Japan.  
Email: claudia@med.u-ryukyu.ac.jp

## Funding information

Japan Society for the Promotion of Science, Grant/Award Numbers: 18J10834, 18K07100, 21H02732, 18H02655

## Abstract

Bacterial pathogens have evolved multiple strategies to disassemble epithelial cell apical junctional complexes (AJCs) and infect epithelial cells. Leptospirosis is a widespread zoonotic infection, mainly caused by *Leptospira interrogans*, and its dissemination across host cell barriers is essential for its pathogenesis. However, the mechanism of bacterial dissemination across epithelial cell barriers remains poorly characterised. In this study, we analysed the interaction of *L. interrogans* with renal proximal tubule epithelial cells (RPTECs) and found that at 24 hr post-infection, *L. interrogans* remain in close contact with the plasma membrane of the RPTEC by extracellularly adhering or crawling. *Leptospira interrogans* cleaved E-cadherin and induced its endocytosis with release of the soluble N-terminal fragment into the extracellular medium. Concomitantly, a gradual decrease in transepithelial electrical resistance (TEER), mislocalisation of AJC proteins (occludin, claudin-10, ZO-1, and cingulin) and cytoskeletal rearrangement were observed. Inhibition of clathrin-mediated E-cadherin endocytosis prevented the decrease in TEER. We showed that disassembly of AJCs in epithelial cells and transmigration of bacteria through the paracellular route are important for the dissemination of *L. interrogans* in the host.

## KEYWORDS

apical junctional complex, *Leptospira interrogans*, renal epithelial cells

## 1 | INTRODUCTION

The apical junctional complex (AJC) encircles pairs of neighbouring epithelial and endothelial cells to create an adhesive network and maintain barrier integrity (Rusu & Georgiou, 2020). Two important types of intercellular junctions, the tight junction (TJ) and adherens

junction (AJ), are spatiotemporally regulated to form the AJC (Rusu & Georgiou, 2020). AJs are composed of cadherins, which are transmembrane proteins that participate in homophilic interactions with cadherins located on adjacent cells. TJs are composed of transmembrane proteins such as occludin, claudin, and junction adhesion molecule (JAM) proteins (Zihni, Mills, Matter, & Balda, 2016). The

This is an open access article under the terms of the Creative Commons Attribution-NonCommercial License, which permits use, distribution and reproduction in any medium, provided the original work is properly cited and is not used for commercial purposes.

© 2021 The Authors. *Cellular Microbiology* published by John Wiley & Sons Ltd.

formation and stability of the AJCs depend on the transmembrane proteins that anchor it to the actin cytoskeleton through scaffolding proteins (such as ZO-1 and cingulin) and coordinated signalling pathways involving the Rho family of small GTPases (McCormack, Welsh, & Braga, 2013).

Bacterial pathogens have evolved strategies to hijack AJC proteins in order to disturb this complex stability, and translocate through endothelial and epithelial cells to establish an infection (Drolić & Bhunia, 2019; Huber, 2020; Martens, Neumann, & Desai, 2018). Thus, altering the integrity of AJCs via mechanisms such as transcriptional and post-transcriptional downregulation, bacterial or host protease-mediated cleavage, perturbation of host signalling pathways, disruption of the cytoskeleton, and mislocalisation of AJC proteins is important for the dissemination and pathogenesis of several pathogens (Devaux, Mezouar, & Mege, 2019; Singh et al., 2018; Tapia, Kralicek, & Hecht, 2017; Ugalde-Silva, Gonzalez-Lugo, & Navarro-Garcia, 2016). Pathogenic *Leptospira*, such as *L. interrogans*, can evade macrophage- and complement-mediated killing after penetrating the skin and translocate across the endothelial barrier of the blood vessels to disseminate hematogenously and reach the target organs, such as the kidney, lung, and liver (Moreno-Torres et al., 2019; Picardeau, 2017; Toma, Okura, Takayama, & Suzuki, 2011). Studies investigating the molecular basis of pathogenic *Leptospira* dissemination have utilised *in vivo* or *in vitro* models and have provided significant insights into the pathogenesis of *L. interrogans*. For example, early studies using a hamster model of infection showed the ability of leptospires to actively penetrate in between renal proximal tubule epithelial cells (RPTECs) via detachment of TJs (van den Ingh & Hartman, 1986). Consistently, subsequent reports on animal infection models showed the presence of leptospires in the intercellular spaces of the liver and lung, suggesting a paracellular route of cellular translocation (Miyahara et al., 2014; Nikaido et al., 2019). However, conflicting reports have stated that *L. interrogans* translocates the cell monolayers via a transcellular pathway, and not through intercellular junctions (Barocchi, Ko, Reis, McDonald, & Riley, 2002; Wunder et al., 2016). Although translational motility is essential to enable *L. interrogans* to transverse tissue barriers (Wunder et al., 2016), additional unidentified mechanisms might also be important for leptospiral transmigration through host cells. Cultured endothelial cells infected with pathogenic *L. interrogans* showed decreased expression and mislocalisation of AJ and TJ proteins as well as changes in the expression of several genes involved in cellular architecture, suggesting that the endothelial barrier damage is mediated by alteration in multiple proteins of the AJC and remodelling of the actin cytoskeleton (Martinez-Lopez, Fahey, & Coburn, 2010; Sato & Coburn, 2017). However, the perturbation in the AJC has yet not been reported in *Leptospira*-infected cultured epithelial cells.

Immunofluorescence analysis of leptospiral kidney colonisation kinetics in a mouse infection model showed that *L. interrogans* attaches to the basal membrane of the RPTECs before translocation into the lumen (Yamaguchi et al., 2018). The number of *L. interrogans*-colonised tubules was limited, suggesting that in each tubule a minimal infective dose is required for bacterial translocation from the basolateral to the apical surface (Yamaguchi et al., 2018). Ratet et al.

also showed leptospiral colonisation in a limited number of tubules using bioluminescent leptospires (Ratet et al., 2014). However, the mechanism by which *Leptospira* reaches the tubular lumen remains unknown. *Leptospira*-host cell interactions have been studied in cultured human kidney epithelial cell lines (Tian et al., 2006) which showed low expression of the AJ protein E-cadherin (E-cad) (Evangelista, Franco, Schwab, & Coburn, 2014; Wieser et al., 2008), a putative leptospiral receptor (Kochi et al., 2019). Since decreased E-cad expression has been documented in the liver of leptospirosis patients (De Brito et al., 2006; De Brito, Silva, & Abreu, 2018), further analysis of the leptospiral-RPTEC interaction in a cell culture model resembling primary cells will contribute to our understanding of the role of E-cad in the pathogenesis of *Leptospira*.

RPTECs immortalised by ectopic expression of the catalytic subunit of telomerase reverse transcriptase (TERT) show the morphological and functional properties of primary renal epithelial cells, such as the formation of TJs, primary cilia, and domes and high expression of E-cad (Aschauer et al., 2013; Shrestha et al., 2017; Wieser et al., 2008). Therefore, RPTEC/TERT cells are a favourable model for studying *Leptospira*-RPTEC interactions. In this study, we used RPTEC/TERT1 cells to show that the pathogenic *Leptospira* disassembles the AJC and that this involves E-cad endocytosis and ROCK-dependent cytoskeletal rearrangement.

## 2 | RESULTS

### 2.1 | *Leptospira interrogans* localised extracellularly after infecting RPTECs

Previous studies have shown that *L. interrogans* translocates cell monolayers without altering the integrity of cell junctions (Barocchi et al., 2002; Wunder et al., 2016). Studies have also reported the presence of leptospires in the intercellular spaces of target organs in animal models of infection (Miyahara et al., 2014; Nikaido et al., 2019; Yamaguchi et al., 2018). To understand these conflicting results, we developed a cell culture system of differentiated RPTECs with the characteristics of primary RPTECs, such as uniform expression of E-cadherin (Figure S1a). The polarity of RPTECs was gauged by the development of a cilium at the apical domain, which was immunostained with anti-acetylated tubulin antibodies (Aschauer et al., 2013) (Figure S1b). To evaluate the infection kinetics in a wide area of the epithelial monolayer, differentiated RPTECs were infected with *L. interrogans* from the basal side, fixed at 6 hr and 24 hr post-infection (p.i.), sectioned and observed by scanning electron microscopy (SEM). We observed that *L. interrogans* were intracellularly localised in RPTEC/TERT1 cells at 6 hr p.i. (Figure 1a). At 24 hr p.i., leptospires were observed in the intercellular space (Figure 1b). Next, to better understand the interaction between pathogenic leptospires and RPTECs at the cellular level, we performed focused ion beam (FIB)-SEM tomography of *L. interrogans*-infected RPTECs at 24 hr p.i. (Kizilyaprak, Daraspe, & Humbel, 2014; Kizilyaprak, Stierhof, & Humbel, 2019). Leptospires were found to be in close contact with

the plasma membrane in the gap between two adjacent cells (Figure 1c–f, Video S1). In proximity to the leptospires, the RPTECs produced plasma membrane protrusions that were connected to the bacteria (Figure 1e). These plasma membrane protrusions were rarely observed in regions without attached bacteria. Leptospire were also detected in vacuoles within the cell (Figure 1c, Video S1). These results suggest that although *L. interrogans* are endocytosed by RPTECs, at 24 hr p.i., a bacterial population remained extracellularly and translocated the cell monolayer through the paracellular route. The intracellular bacteria might either translocate through the transcellular route or might be degraded in a defence response of the epithelial cell.

## 2.2 | *Leptospira interrogans* induces a decrease in the transepithelial electrical resistance (TEER) and transmigrates through the RPTEC monolayer

To better understand the bacterial dynamics in close contact with the plasma membrane, the fractions of pathogenic *L. interrogans* and non-

pathogenic *L. biflexa* that were adhered or crawled on the plasma membrane were quantified (Xu, Koizumi, & Nakamura, 2020). At 2 hr p.i., the percentage of *L. interrogans* adhering (~22%) was not significantly different than percentage of *L. biflexa* (~16%). However, for *L. interrogans*, the bacterial population interacting with the plasma membrane gradually increased during the course of infection, reaching ~30% (adhering) and ~20% (crawling) of the total bacterial population at 24 hr p.i., which was significantly different from the percentages of *L. biflexa* (Figure 2a). The interactions of *L. biflexa* with the plasma membrane of RPTECs remained unaltered at 24 hr p.i. (~16% adhering, ~6% crawling) (Figure 2a). Dual immunofluorescence analysis of the bacteria and the lysosomal marker LAMP1 at 24 hr p.i. showed the presence of elongated *L. interrogans* that did not colocalise with LAMP1 (Figure 2b). No spirochete-like bacteria were observed in *L. biflexa*-infected RPTECs, suggesting that they poorly adhered to the RPTEC cell surface. We measured TEER to assess whether the epithelial cell monolayer was disturbed by leptospiral attachment (Wieser et al., 2008). TEER gradually started to decrease in *L. interrogans*-infected RPTECs at 6 hr p.i. and was significantly decreased at 24 hr p.i. (~20% of the initial TEER value). In contrast, the TEER of

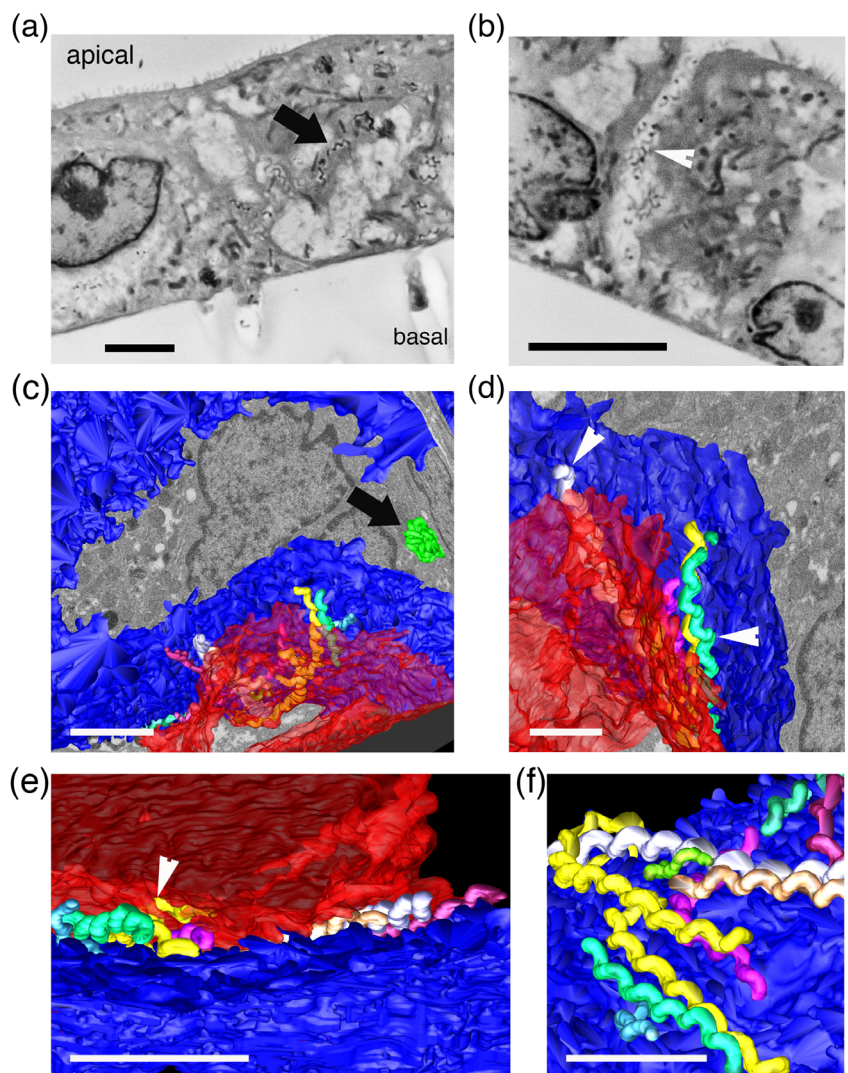


**FIGURE 1** *L. interrogans* localises extracellularly at 24 hr post infection in RPTECs. Infected RPTECs were fixed at 6 hr (a) or 24 hr post infection (b–f) and observed by SEM (a, b) or FIB-SEM (c–f). Intracellular leptospires are indicated by black arrows (a) and (c), and extracellular leptospires are indicated by white arrowheads in (b), (d) and (e). (c–f) Leptospire were artificially differentially coloured to distinguish individual cells, and the cell membranes of adjacent RPTECs were coloured blue and red to depict the location of leptospires in relation to the plasma membrane. (c), (d) and (e) Extracellular leptospires localised in the gap between two adjacent cells in close contact with the plasma membrane (white arrowheads). (f) The red cell membrane of an adjacent cell was removed from the image to show the attachment of leptospires to the surface of the blue cell and that they are in close contact with the membrane protrusions. Scale bars: 5  $\mu\text{m}$  for (a) and (b), 2  $\mu\text{m}$  for (c)–(f)

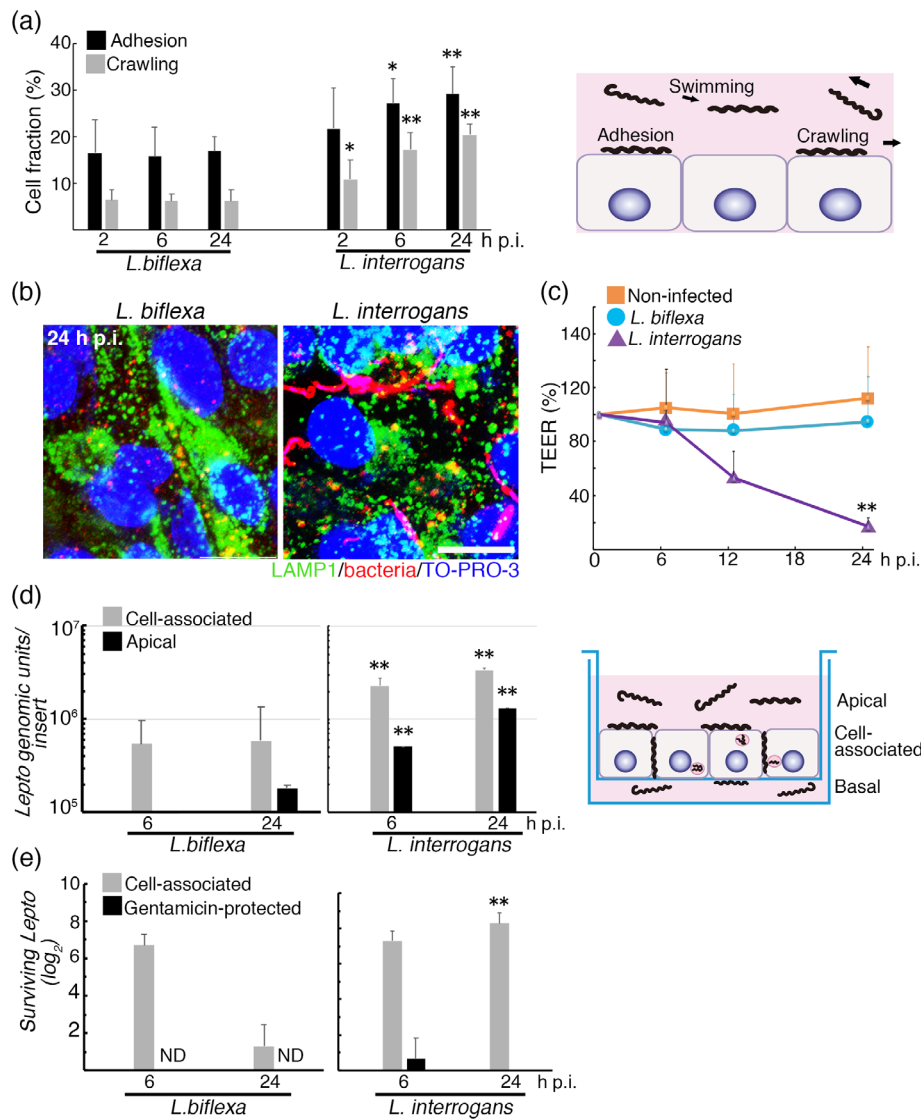


**FIGURE 2** Analysis of the dynamics of bacteria in close contact with the RPTEC plasma membrane. RPTECs were infected with either *L. biflexa* or *L. interrogans* and (a) the fractions of individual *Leptospira* cells adhering and crawling were quantified. The values are expressed as the means  $\pm$  SD of  $\sim$ 2,000 leptospiral cells measured at each time point in randomly selected fields in three independent experiments. A schematic diagram showing *Leptospira* adhering, crawling and swimming is presented on the right. (b) Representative confocal images showing the infected-RPTECs at 24 hr post infection. Bacteria were stained with a Cy3-labelled anti-*Leptospira* antibody (red) and LAMP-1 with a Alexa Fluor 488-labelled antibody (green). The cell nuclei were counterstained with TO-PRO-3 (blue). Scale bar: 10  $\mu$ m. (c) Monolayer integrity was evaluated by measuring TEER. The values are the mean  $\pm$  SD of four independent experiments. (d) Quantification of bacterial DNA at the apical side or cell-associated DNA by qPCR. The values are the mean  $\pm$  SD of three independent Transwells. A schematic diagram showing cell-associated and apical *Leptospira* is presented on the right. (e) Cell-associated and gentamicin-protected *Leptospira* was quantified by the gentamicin protection assay. The cell-associated *Leptospira* was recovered from the infected RPTECs in antibiotic-free medium and the gentamicin-protected *Leptospira* from the infected RPTECs in gentamicin supplemented medium. The values are the mean  $\pm$  SD of three independent Transwells. ND: leptospires not detected by dark field microscope. \*  $p < .05$  and \*\*  $p < .01$  versus *L. biflexa* at the same time point in the same cell fraction (a), or cell compartment (d)

*L. biflexa*-infected RPTECs was not significantly different from that of non-infected RPTECs ( $\sim$ 100% of the initial TEER; Figure 2c). To better define the time-course of the infection and determine if *L. interrogans* can translocate to the apical side, we quantified cell-associated and apically translocated bacterial DNA using real-time PCR (qPCR). *Leptospira interrogans* DNA was detected on the apical side at 6 hr p.i. when TEER had not decreased, and at 24 hr p.i. This

was further confirmed by the presence of motile spirochetes using dark-field microscopy (Figure 2d, Figure S2). Apically translocated *L. biflexa*-DNA was detectable at 24 hr p.i.; however, spirochetes were not observed by dark-field microscopy (Figure S2). Cell-associated bacterial DNA was significantly higher in *L. interrogans*-infected RPTECs than that in *L. biflexa*-infected RPTECs at 6 hr and 24 hr p.i. (Figure 2d). The cell-associated fraction of bacteria included

internalised bacteria and pericellular bacteria that were attached and/or were dynamically transmigrating through the plasma membrane (Figure 2d). The gentamicin protection assay used to quantify cell-associated and the gentamicin-protected (intracellularly surviving) leptospire, showed that in *L. biflexa*-infected RPTECs cell-associated leptospire decreased during the course of infection, while in *L. interrogans*-infected RPTECs, cell-associated leptospire remained pericellular (gentamicin-susceptible) at 24 hr p.i. (Figure 2e). The low recovery of surviving leptospire after gentamicin treatment (Figure 2e) suggested that morphologically intact intracellular leptospire detected by imaging techniques (Figure 1a,c) might be killed in a host defence response, and/or might become gentamicin sensitive due to RPTEC plasma membrane disruption by leptospiral pore-forming toxins (Picardeau, 2017). Together, these results indicate that *L. interrogans* disrupts the integrity of the cell monolayer and transmigrates from the basolateral to the apical surface of polarized RPTECs. Transmigration might occur mainly through the transcellular pathway at the early stage of infection (~6 hr p.i.) and by the paracellular pathway at later stages of infection (~24 hr p.i.).

### 2.3 | *Leptospira interrogans* induces E-cadherin cleavage and mislocalisation of apical junctional complex transmembrane proteins

Organisation and maintenance of the monolayer integrity of epithelial cells require functional AJCs, with E-cad as a key molecule. Structurally, E-cad consists of five extracellular domains, a single transmembrane domain and an intracellular domain (van Roy & Berx, 2008). Sato and Coburn have reported that *L. interrogans* perturbs the expression and morphology of AJ proteins in endothelial cells (2017); thus, we hypothesized that *L. interrogans* might also similarly inhibit the expression of AJC proteins in RPTECs. Therefore, we comprehensively analysed the changes in transcript profiles in response to *L. interrogans* infection to understand *L. interrogans*-induced disruption in the RPTEC monolayer. We subjected non-infected and *L. interrogans*-infected RPTECs to RNA-sequencing (RNA-seq) and identified 86 downregulated genes and 54 upregulated genes with a fold change >2 ( $q$  value <0.005; Tables S1 and S2). However, none of the AJC-associated structural proteins showed a transcription decrease (Table S1). Interestingly, *myosin 7b* (*Myo7b*), which codes for a component of the intermicrovillar adhesion complex (Weck, Crawley, Stone, & Tyska, 2016), showed a 4.66-fold decrease in expression and was among the top 10 most downregulated genes (Table S1).

Since AJC disassembly might be induced without affecting transcript levels, we next investigated the expression of E-cad in infected RPTECs by immunoblot using an antibody directed to the extracellular N-terminal fragment (NTF) (soluble domains of E-cadherin, S-E-cad). We did not detect a significant decrease in the expression level or the molecular weight of full-length E-cad (E-cad-FL; Figure 3a,b). Pathogens can induce cleavage of E-cad either by bacterial or eukaryotic proteases to favour bacterial invasion and transmigration (Backert,

Bernegger, Skórko-Glonek, & Wessler, 2018; Devaux et al., 2019). Thus, we hypothesized that E-cad might be cleaved during *L. interrogans* infection without causing a detectable decrease in the amount of E-cad-FL, and analysed the extracellular soluble proteins. We observed the presence of an 80 kDa E-cad-fragment, which corresponds to S-E-cad, on the basal side of both *L. biflexa* and *L. interrogans*-infected RPTECs (Hoy et al., 2010). In *L. interrogans*-infected RPTECs, S-E-cad was also observed on the apical side (Figure 3a). Since cleavage of the extracellular NTF of E-cad results in the formation of non-trans-interacting E-cad, which is preferentially internalised (Cruz et al., 2015), we next investigated the localisation of E-cad at the cellular level by confocal microscopy using antibodies directed to the E-cad C-terminal fragment. E-cad levels at the plasma membrane were decreased in *L. interrogans*-infected RPTECs, but not in *L. biflexa*-infected RPTECs, compared to that in non-infected (n.i.) cells (Figure 3c). This result suggested that in *L. interrogans*-infected RPTECs, additional mechanisms, such as degradation of AJC components by proteases, act together with E-cad cleavage to induce a decrease in E-cad levels at the plasma membrane.

We considered the possibility that TJ proteins are cleaved during *L. interrogans* infection of RPTEC. Since occludin is involved in the maintenance and regulation of the paracellular barrier, we immunoblotted for occludin to assess the integrity of the paracellular barrier. We did not observe occludin cleavage in *L. interrogans*-infected cells, and occludin protein levels were similar to that in non-infected and *L. biflexa*-infected RPTECs (Figure 3a,b). However, we observed that occludin was displaced from the membrane of *L. interrogans*-infected RPTECs, but not the membrane of *L. biflexa*-infected RPTECs (Figure 3c). Analysis of infected RPTECs by FIB-SEM at 3 hr p.i. showed an electron-dense area between adjacent cells corresponding to the AJC and *L. interrogans* penetrating the intercellular side (Figure S3). Considering these results, we analysed the localization of the transmembrane protein claudin, which is polymerised to form TJ strands and can be observed as contact points between two neighbouring epithelial cells by transmission electron microscopy (TEM) (Tsukita, Tanaka, & Tamura, 2019). The TJ strands were still present at 6 hr p.i. when *L. interrogans* was localised both, intracellularly and pericellularly (Figure 4a,b). At 24 hr p.i., TJ strands were absent, and leptospire were observed in the paracellular space and on the apical side of RPTECs (Figure 4c). Immunofluorescence of claudin-10 suggested intact TJ strands in non-infected cells, but claudin-10 was also displaced from the TJs of *L. interrogans*-infected RPTECs (Figure 4d). Collectively, these results show that although E-cad cleavage is induced by both *L. biflexa* and *L. interrogans*, the mislocalisation of TJ transmembrane proteins are *L. interrogans*-specific events.

### 2.4 | *Leptospira interrogans* induces the mislocalisation of AJC scaffold proteins and the rearrangement of F-actin

Since *L. interrogans* perturbed the localisation of transmembrane TJ proteins, we next analysed the scaffold proteins ZO-1 and cingulin.

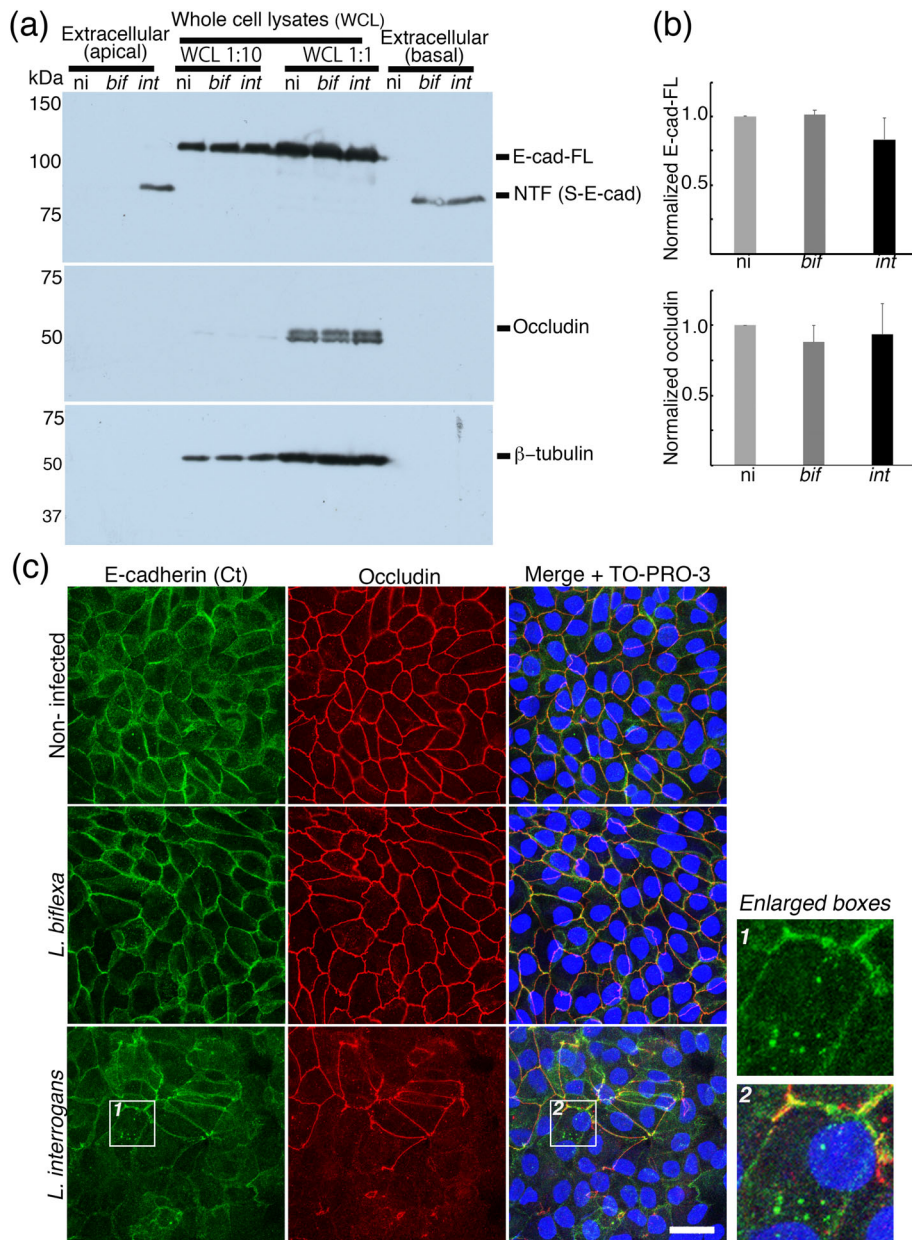


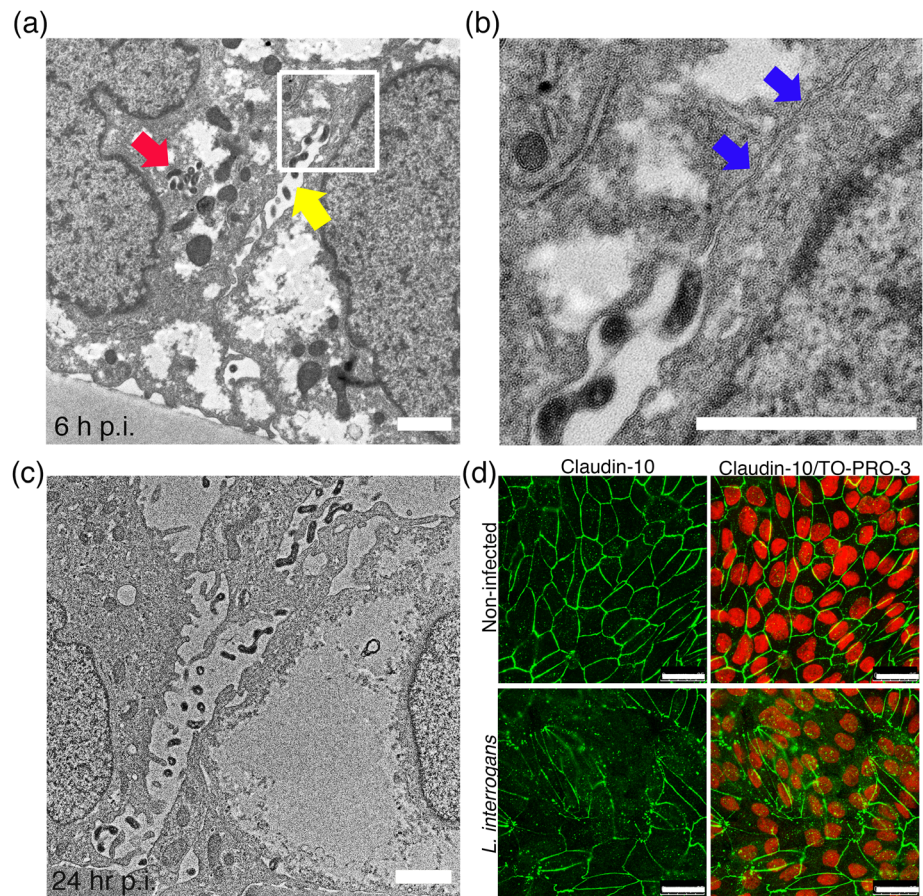
**FIGURE 3** *L. interrogans* induces E-cadherin cleavage and mislocalisation of apical junctional complex transmembrane proteins. RPTECs were infected either with *L. biflexa* (bif) or *L. interrogans* (int) and compared with non-infected (ni) RPTECs at 24 hr post infection. (a) Immunoblotting for the AJC proteins E-cadherin or occludin in whole cell lysates (WCLs), undiluted whole cell lysates (WCL 1:1), 10-fold diluted whole cell lysates (WCL 1:10), and extracellular compartments (apical and basal).  $\beta$ -Tubulin was used as a loading control. (b) Normalised levels of apical junctional proteins. Each bar represents mean  $\pm$  SD of three independent experiments. (c) Representative confocal images of non-infected and infected-RPTECs. E-cadherin was stained with an Alexa Fluor 488-labelled antibody (green), occludin was labelled with a Cy3-labelled antibody (red), and the cell nuclei were counterstained with TO-PRO-3 (blue). Scale bar: 20  $\mu$ m. Enlarged boxes showing internalised transmembrane proteins are shown on the right

Scaffold proteins link transmembrane TJ/AJ proteins to the cytoskeleton, enabling efficient regulation of signals originating from intercellular junctions (Citi, Pulimeno, & Paschoud, 2012). Immunofluorescence analysis showed that ZO-1 and cingulin were displaced from the AJCs of *L. interrogans*-infected RPTECs (Figure 5a).

Cingulin binds to ZO-1 and actin through its N-terminal globular head domain and in well-established TJ complexes (Figure 8), and it is detected in the insoluble fractions during protein extraction because of its strong association with the cytoskeleton (Schossleitner et al., 2016). We estimated cingulin levels in total protein extracts of non-infected, *L. biflexa*-infected, and *L. interrogans*-infected RPTECs by immunoblotting of the soluble and insoluble fractions after cell lysis. The main cellular pool of cingulin was detected in the insoluble fractions of non-infected and infected RPTECs. However, it was detected significantly higher in the soluble fraction of *L. interrogans*-

infected RPTECs at 24 hr p.i., suggesting its dissociation from the cytoskeleton (Figure 5b,c). In *L. biflexa*-infected RPTECs, cingulin was mainly detected in the insoluble fraction, even at 48 hr p.i. (Figure 5b). Next, to clarify if cingulin solubilisation in *L. interrogans*-infected RPTECs was induced by a rearrangement of the cytoskeleton, we focus on F-actin organisation. *Leptospira interrogans* caused rearrangement of the actin cytoskeleton, as assessed by rhodamine-phalloidin staining (Figure 5d). The most striking feature was the decrease in the circumferential F-actin belt and the appearance of F-actin-lined vacuoles, which did not colocalise with bacteria (Figure 5d). Marinho et al. reported by using an animal model that *L. interrogans* induces cell death of renal epithelial cells in later phases of infection (Marinho, Táparo, Oliveira-Júnior, Perri, & Cardoso, 2015). To investigate if F-actin disruption and AJC disassembly reflects a consequence of cell death, cell viability, and DNA

**FIGURE 4** *L. interrogans* induces mislocalisation of claudin-10 and disruption of TJ strands. RPTECs were infected with *L. interrogans*, and then fixed and processed for TEM or immunofluorescence. (a) Electron micrographs showing intact tight junction strands and intracellularly located (red arrow) and paracellularly located (yellow arrow) *L. interrogans* at 6 hr post infection (p.i.). (b) A higher magnification of the inset in (a), showing the tight junction strands, which are indicated by blue arrows. (c) Electron micrograph showing disrupted TJ strands and paracellularly located *L. interrogans* and on the apical side at 24 hr p.i. (d) Representative confocal images of non-infected and infected-RPTECs at 24 hr p.i. Claudin-10 was stained with an Alexa Fluor 488-labelled antibody (green) and the cell nuclei were counterstained with TO-PRO-3 (red). Scale bars: 1  $\mu\text{m}$  for (a)–(c), 25  $\mu\text{m}$  for (d)



fragmentation were evaluated in infected RPTECs using cisplatin as a positive control of cell death-inducer of RPTECs (Sallustio et al., 2013). There was not a significant decrease in cell viability in *L. interrogans*-infected RPTECs (Figure 5e), although a slight increase (~1.4%) of TUNEL positive cells was detected in *L. interrogans*-infected RPTECs (Figure 5f, Figure S4). Taken together, these results suggest that *L. interrogans* induces mislocalisation of TJ scaffolding proteins and rearrangement of the cytoskeleton, inducing the dissociation of cingulin from F-actin independent of cell death induction.

## 2.5 | The rho-associated kinase (ROCK) signalling pathway and clathrin-mediated E-cad endocytosis are involved in AJC disassembly

Cingulin-mediated recruitment of the guanine nucleotide exchange factor H1 (GEF-H1) at TJs prevents RhoA signalling activation in polarised epithelial cells (Figure 8) (Aijaz, D'Atri, Citi, Balda, & Matter, 2005; Citi et al., 2009). Furthermore, ROCK signalling is involved in cytoskeletal rearrangement and disruption of homotypic E-cadherin interactions between neighbouring cells, inducing AJC disassembly (Samarin, Ivanov, Flatau, Parkos, & Nusrat, 2007). Thus, we investigated the possibility that the RhoA/ROCK signalling pathway is activated during the disassembly of AJCs. Selective inhibition of

ROCK with Y27632 and H1152 inhibited the formation of F-actin-lined vacuoles and partially reduced the number of *L. interrogans*-infected cells with disassembled AJCs, without preventing the TEER decrease (Figure 6a,b, Figure S5).

E-cad within the cadherin-catenin complex interacts with F-actin and microtubules, and creates a tightly regulated signalling platform that physically links the AJs to the cytoskeleton (Rusu & Georgiou, 2020) (Figure 8). The dissociation of p120 catenin from the AJC decreases membrane stability of E-cad (Kourtidis, Ngok, & Anastasiadis, 2013) and induces clathrin-mediated endocytosis (CME) of E-cad, which requires the vesicular coat protein, clathrin, and the GTPase dynamin (Cruz et al., 2015). We found that in *L. biflexa*-infected RPTECs, p120 catenin localised at the cell-cell junction, while *L. interrogans* induces aberrant p120 catenin localization in infected RPTECs (Figure S6). Thus, we hypothesized that in *L. interrogans*-infected RPTECs E-cad endocytosis is enhanced due to the formation of non-trans-interacting E-cad because of NTF cleavage, decreased interaction of E-cad with actin filament and/or the aberrant p120 catenin localization. To test this, we used dynasore, an inhibitor of dynamin (Macia et al., 2006), and evaluated monolayer integrity. Addition of dynasore 1 hr before infection, inhibited *L. interrogans*-induced effects, such as TEER decrease, E-cad and occludin mislocalisation, F-actin rearrangement and AJC disassembly (Figure 6a–c, Figure S7a,b). RPTEC pretreatment with dynasore did

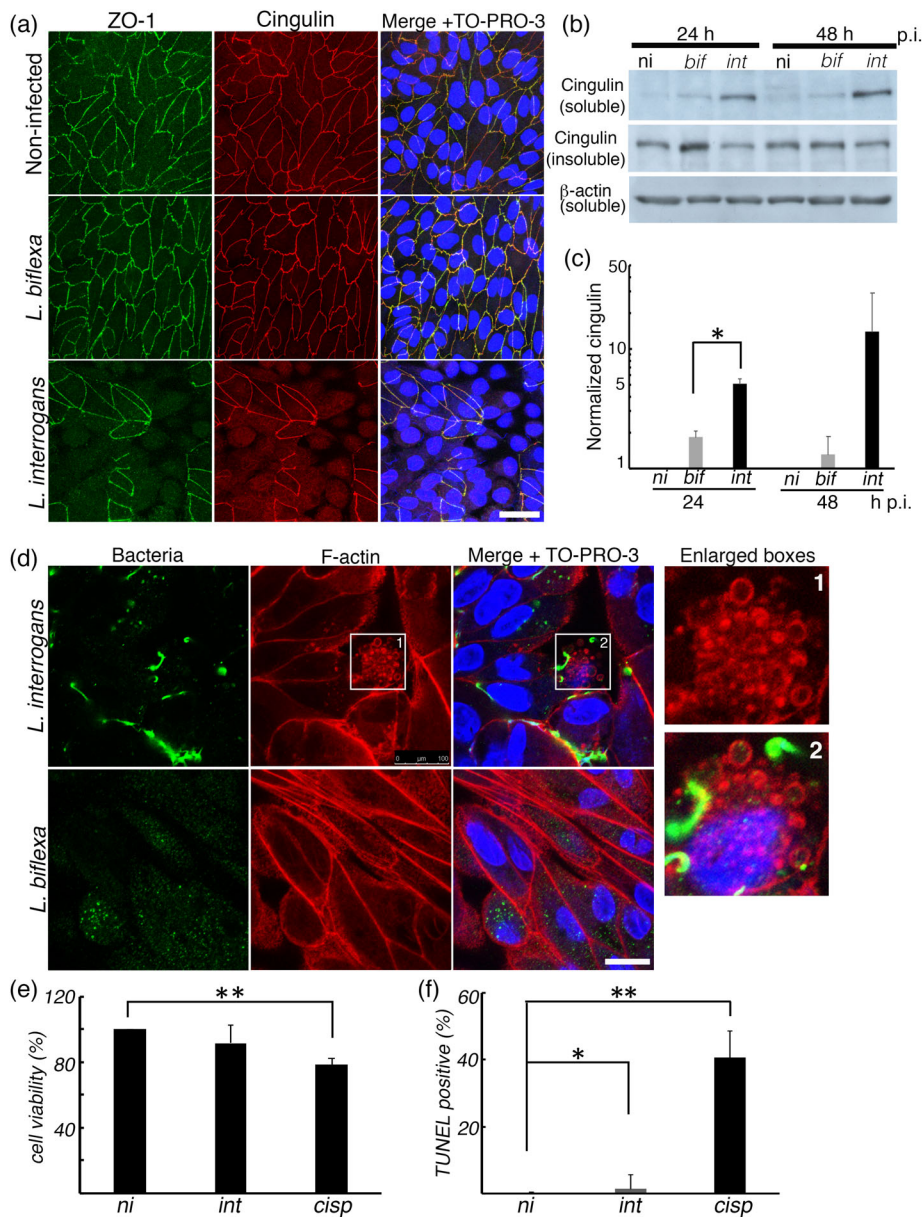


**FIGURE 5** *L. interrogans* induces mislocalisation of scaffold proteins and rearrangement of F-actin. RPTECs were infected either with either *L. biflexa* (*bif*) or *L. interrogans* (*int*), and then processed for immunofluorescence, immunoblotting, cell viability assay or TUNEL staining. (a) Representative confocal images showing mislocalisation of scaffold proteins. ZO-1 was stained with an Alexa Fluor 488-labelled antibody (green), cingulin was stained with a Cy-3-labelled antibody (red); and the cell nuclei were counterstained with TO-PRO-3 (blue). Scale bar: 20  $\mu$ m. (b) Immunoblotting of the soluble and insoluble fractions after cell lysis of non-infected (ni) and *L. biflexa*- or *L. interrogans*-infected cells at 24 hr and 48 hr post infection.  $\beta$ -actin was used as a loading control. (c) Normalised levels of cingulin (soluble). (d) Representative confocal images showing rearrangement of F-actin. Bacteria were stained with an Alexa Fluor 488-labelled antibody (green), F-Actin was stained with rhodamine-phalloidin (red), and the cell nuclei were counterstained with TO-PRO-3 (blue). Scale bar: 10  $\mu$ m. (e) Cell viability determined by crystal violet assay. Cisplatin (*cisp*) was used as a positive control of cell death induction. (f) Quantification of TUNEL positive cells (see also Figure S4). Each bar represents mean  $\pm$  SD of three independent experiments. \*  $p < .05$  and \*\*  $p < .01$

not significantly inhibit the translocation of leptospire to the apical side, but cell-associated *L. interrogans* was significantly decreased at 24 hr p.i. (Figure 6d,e; Figures S7a and S8). These results suggested that although dynasore inhibited E-cad endocytosis, the “off-target effects” of this inhibitor (Preta, Cronin, & Sheldon, 2015) might induce increase transcellular leptospiral transmigration and interfere with *L. interrogans*–plasma membrane interactions. To strengthen our hypothesis that E-cad endocytosis is involved in AJC disassembly, we investigated the effect of Pitstop2, a clathrin inhibitor (Bryant & Stow, 2004), on *L. interrogans*-induced AJC disassembly. Furthermore, we tried to avoid inhibitors “off-target effects” during the initial leptospiral/RPTEC interactions and modified our protocol by adding the inhibitors at 2 hr post infection. Dynasore and Pitstop2 prevented TEER decrease and AJC disassembly induced by *L. interrogans* infection (Figure 7a–c). The modified protocol showed that, at 6 hr p.i.,

apical leptospiral DNA was significantly increased in dynasore-treated RPTECs (Figure 7d). On the other hand, apical leptospiral DNA was significantly decreased in Pitstop2-treated RPTECs at 24 hr post infection. Pitstop2 did not decrease cell-associated *L. interrogans*, but bacterial association to the basal membrane was observed by immunofluorescence at 24 hr p.i. (Figures S9). The presence of occludin at AJC without E-cad suggested that E-cad endocytosis preceded occludin displacement from the membrane (Figure 7c, white arrows). The percentage of RPTECs that showed displacement of E-cad from the cell membrane was significantly higher than those showed occludin displacement at 14 hr p.i. (Figure S10).

Collectively, these results suggested that E-cad endocytosis and F-actin rearrangement induce AJC disassembly to expose cell–cell junction membrane enabling the transmigration of crawling *L. interrogans* through the paracellular route.



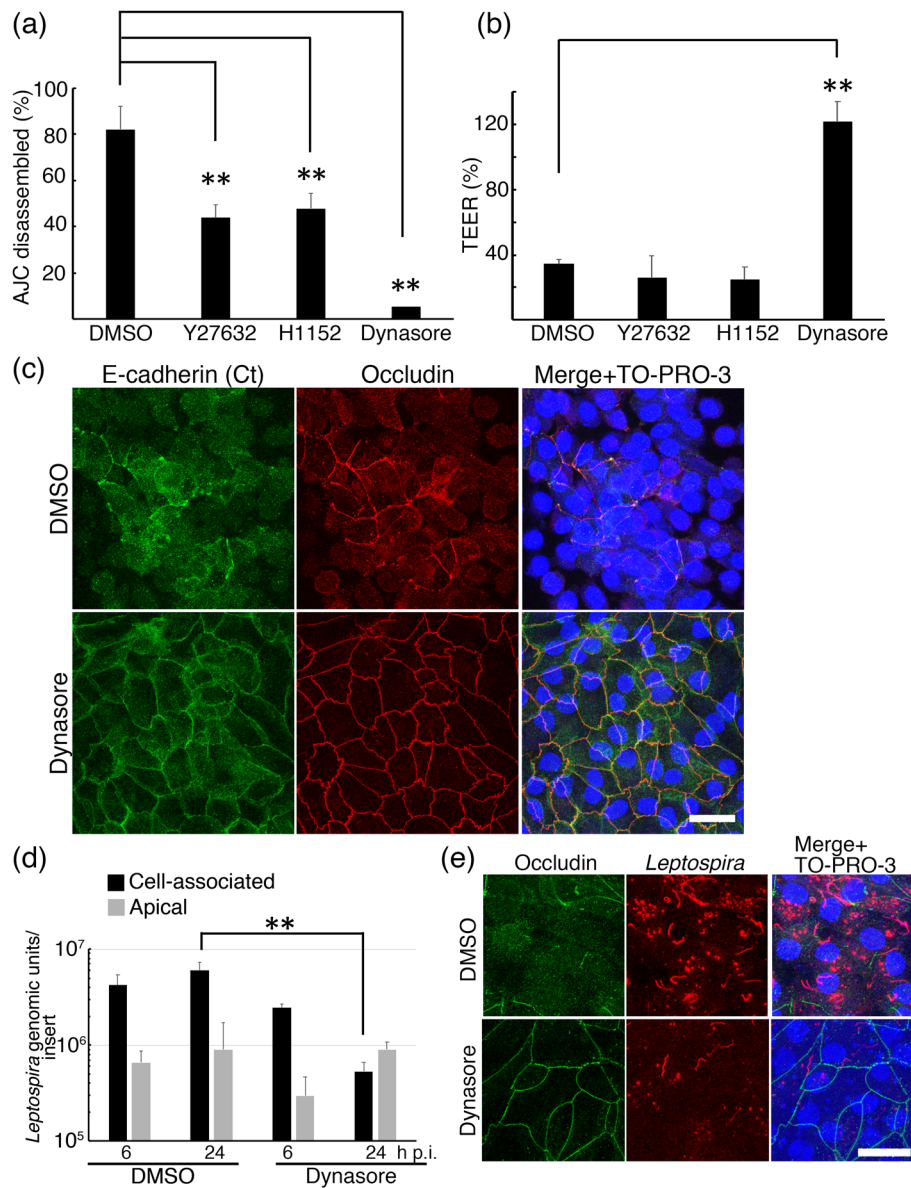


**FIGURE 6** The ROCK signalling pathway and clathrin-mediated E-cad endocytosis are involved in AJC disassembly. (a) RPTECs were pre-treated with Y27632 or H1152 (ROCK inhibitors), dynasore (dynamin inhibitor), or DMSO (as control) from 1 hr before infection; infected with *L. interrogans*; and the percentage of cells showing marked AJC disassembly were quantified after occludin immunofluorescence staining at 24 hr p.i. (see also Figure S5). The percentages are based on counts of at least 200 cells, and the values are presented as the mean  $\pm$  SD of three independent experiments. (b) RPTECs were pre-treated and infected as in (a), and monolayer integrity was evaluated by measuring TEER at 24 hr post infection. (c) Representative confocal images showing the inhibition of AJC disassembly by dynasore pretreatment in *L. interrogans*-infected RPTECs. E-cad was stained with an Alexa Fluor 488-labelled antibody, occludin with a Cy-3-labelled antibody, and the cell nuclei were counterstained with TO-PRO-3 (blue). (d) Quantification of bacterial DNA at the apical side or cell-associated by qPCR after *L. interrogans* infection of RPTECs treated with dynasore or DMSO as control. Data are representative of one experiment with three independent Transwells and are shown as the mean  $\pm$  SD. (e) Representative confocal images showing cell-associated leptospires at 24 hr p.i. in DMSO or dynasore-pretreated RPTECs. Occludin was stained with an Alexa Fluor 488-labelled antibody (green), bacteria with a Cy3-labelled anti-*Leptospira* antibody (red) and the cell nuclei were counterstained with TO-PRO-3 (blue). Scale bars: 20  $\mu$ m. \*\* $p < .01$

### 3 | DISCUSSION

*Leptospira interrogans* causes a widespread life-threatening infection called leptospirosis. Several extracellular virulence factors and motility are associated with its virulence and are essential for traversing tissue barriers (Picardeau, 2017; Wunder et al., 2016; Xu et al., 2020).

However, the detailed mechanisms of bacterial dissemination across epithelial cells remain poorly characterised. In this study, we demonstrated that *L. interrogans* induces displacement of AJC-associated transmembrane and scaffold proteins, resulting in AJC disassembly and opening of the paracellular route for the transmigration of bacteria across RPTECs. Our results indicate that *L. interrogans* induces AJC

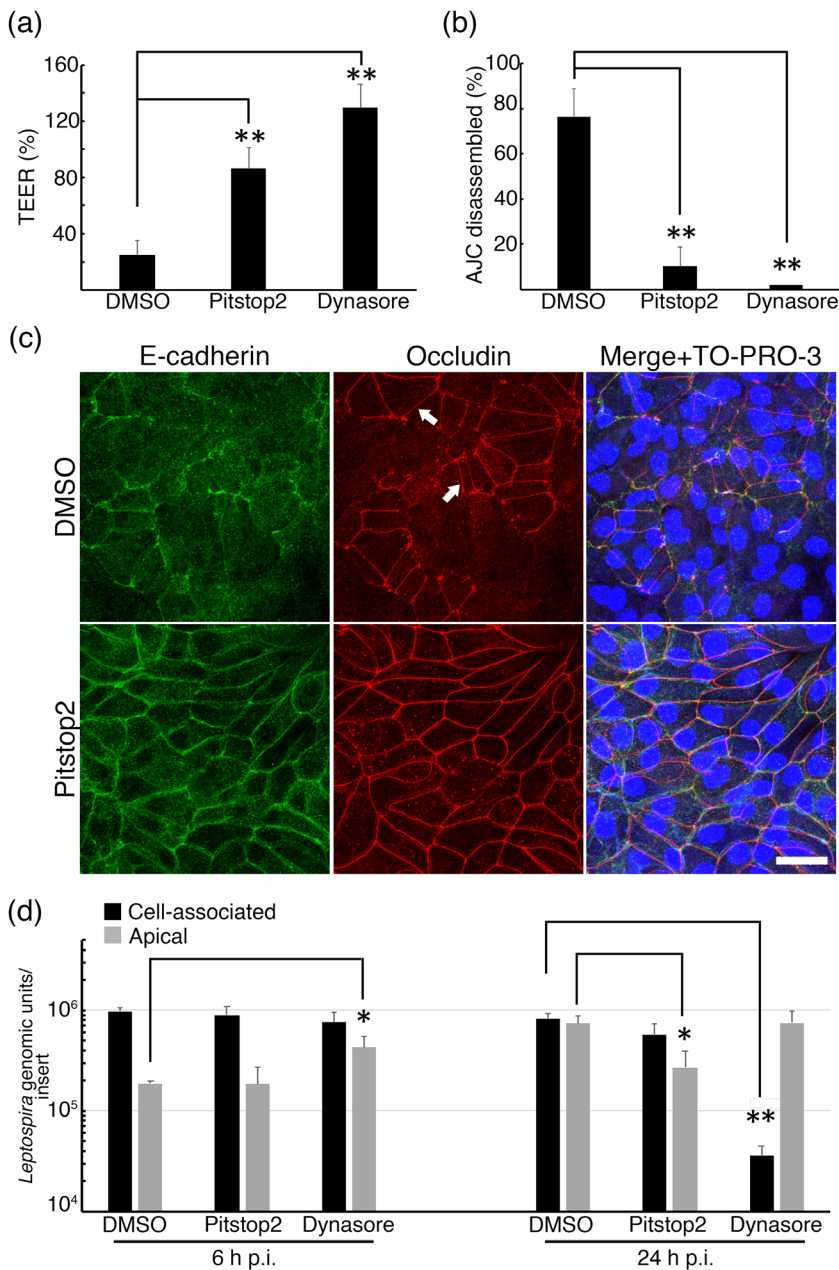


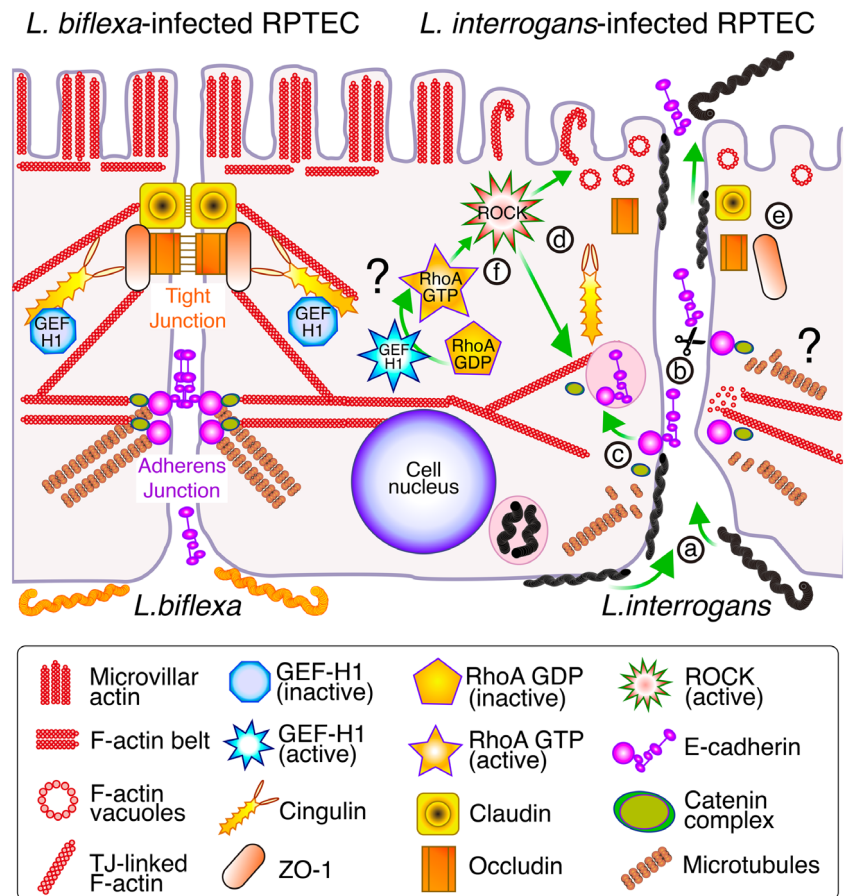
**FIGURE 7** Pitstop2 prevents paracellular *L. interrogans* transmigration. (a) RPTECs were treated with dynasore or Pitstop2 (E-cad endocytosis inhibitors), or DMSO (as control) from 2 hr p.i. and infected with *L. interrogans*. (a) Monolayer integrity was evaluated by measuring TEER at 24 hr post infection. (b) RPTECs were treated and infected as in (a) and the percentage of cells showing marked AJC disassembly were quantified after immunofluorescence staining of occludin. The percentages are based on counts of at least 200 cells, and the values are presented as the mean  $\pm$  SD of three independent experiments. (c) Representative confocal images showing infected RPTECs. E-cad was stained with an Alexa Fluor 488-labelled antibody, occludin with a Cy-3-labelled antibody, and the cell nuclei were counterstained with TO-PRO-3 (blue). Occludin localised at membranes where E-cad had been displaced from the membrane (white arrows). Scale bar: 20  $\mu$ m. (d) Quantification of bacterial DNA at the apical side or cell-associated DNA by qPCR. Data are shown as the mean of three independent Transwells and  $\pm$ SD. \* $p < .05$  and \*\* $p < .01$

disassembly through several mechanisms. Specifically, we found that *L. interrogans* induces shedding of the S-E-cad fragment into the extracellular milieu, ROCK-dependent cytoskeleton rearrangement and CME of E-cad. Displacement of the E-cad pool from the membrane of *L. interrogans*-infected RPTECs alters cell-cell adhesion giving rise to dynamic changes in adhesion between epithelial cells sufficient to drive AJC disassembly and extrusion of the adhesion-compromised cells (Grieve & Rabouille, 2014). Since *L. biflexa* also induces shedding of S-E-cad without displacement of the AJC from the membrane, our results suggest that the levels of E-cad displaced from the cell membrane should be higher than the steady-state levels of E-cad maintained by the synthesis of new protein and recycling of old proteins (Kowalczyk & Nanes, 2012). Thus, cleavage of E-cad seems to be counteracted by E-cad turnover in *L. biflexa*-infected RPTECs, as

the membrane localization of E-cad and TEER in infected cells were similar to those in non-infected cells. In *L. interrogans*-infected RPTECs, E-cad membrane localization and TEER were severely decreased due to the induction of E-cad endocytosis (Figure 8). The intracellular food-borne pathogen *Listeria monocytogenes* also activates E-cad endocytosis to accelerate bacterial invasion of the intestine (Pentecost, Kumaran, Ghosh, & Amieva, 2010). Thus, our results show that extracellular bacterial pathogens as well as intracellular pathogens can induce E-cad endocytosis to disturb cell-cell interactions and disseminate in the host.

Cleavage of E-cad can be induced by exposure to lipopolysaccharide (LPS), pro-inflammatory cytokines, or by host and bacterial proteases. A number of pathogens have reported to secrete bacterial serine proteases of the HtrA family, which promote the shedding of the S-E-

**FIGURE 8** Proposed model of AJC disassembly by *L. interrogans* RPTEC infection. (a) Attachment to and crawling of *L. interrogans* on the plasma membrane, (b) cleavage of E-cad, (c) clathrin-mediated internalisation of E-cad and (d) ROCK-dependent cytoskeleton rearrangement act together to disrupt the epithelial cell monolayer. These events are concomitant with the displacement of (e) the TJ membrane and scaffold proteins (occludin, claudin-10, cingulin and ZO-1) from the membrane. Further (f) activation of the RhoA/ROCK-signalling pathway, due to the release of cingulin from the cytoskeleton and failure to inhibit GEF-H1 at TJs, or dysregulation of an unidentified pathway might enhance AJC disassembly



cad domain, enabling tissue invasion and transmigration (Backert et al., 2018; Devaux et al., 2019). *Leptospira interrogans* encodes Htr-A homologues (Daroz, Fernandes, Teixeira, & Nascimento, 2020; Satou et al., 2015) that might play a role in E-cad cleavage. E-cad has been reported as a putative leptospiral receptor (Eshghi et al., 2019; Kochi et al., 2019), but the binding domain of E-cad has not been determined, and further studies are needed to determine the importance of E-cad cleavage for the retrieval of host cell binding sites. Interestingly, a leucine-rich repeat (LRR) protein from *Leptospira santarosai* (LRR20) binds to the NTF of E-cad and induces the expression of neutrophil gelatinase associated lipocalin (NGAL) in renal HK2 cells (Hsu et al., 2020). NGAL contributes to the innate immunity of the host by reducing iron concentration to limit bacterial growth (Forster et al., 2017). Thus, reducing the expression of E-cad at cell surface might be a bacterial strategy for decreasing NGAL expression and evading the host defence response. Although the role of S-E-cad in *L. interrogans* infection is unknown, an E-cad-binding LRR protein (LIC10831) that is secreted by *L. interrogans* into the extracellular milieu has been identified, and it might counteract the biological effects of S-E-cad (Eshghi et al., 2019). The surface protein internalin A of *L. monocytogenes* binds to the NTF of E-cad and shedding of S-E-cad in *L. monocytogenes* infected cells was proposed as an innate form of pathogen defence by acting as a decoy receptor (da Silva Tatley, Aldwell, Dunbier, & Guilford, 2003).

Previous studies that analysed *L. interrogans* translocation through cell monolayers focused on intracellular bacteria and the bacteria that are released into the medium after translocation and concluded that bacterial transmigration through the transcellular pathway (Barocchi et al., 2002). In agreement with previous studies, we found that at the early stage of infection (~6 hr p.i.), bacteria transmigrated through the monolayer without affecting TEER (Barocchi et al., 2002; Wunder et al., 2016). FIB-SEM tomography of *L. interrogans* interacting with RPTECs showed that, at 24 hr p.i., a bacterial population remained extracellularly but in close contact with the plasma membrane of RPTECs. This bacterial population was either adhered to or crawling on the RPTECs. Leptospirae exhibit crawling motility, which allow them to persistently travel long distances over surfaces and they remain attached to the plasma membrane of the tubular lumen to avoid its clearance through the urine in order to establish a kidney infection. Thus, we believe that not only the release of bacteria into the medium, but also the leptospiral association with host cell during and after transmigration are key pathogenic features and warrant evaluation for understanding *L. interrogans* pathogenesis.

The AJC spatiotemporally regulates the activation of Rho family GTPases, and thus the organisation of the cytoskeleton; however, this equilibrium can be perturbed by mechanical stresses and pathological cues (cytokines and bacterial toxins), leading to AJC disruption (Citi, Guerrero, Spadaro, & Shah, 2014). The organisation of the apical actin cytoskeleton in polarized epithelial cells consists of

apical microvillar actin bundles, TJ-linked F-actin, and the circumferential F-actin belt connected to AJs (Figure 8) (Ivanov, Parkos, & Nusrat, 2010). Induction of signalling pathways by inflammatory mediators results in junction disassembly and a consequent decrease in TEER (Ivanov et al., 2010). Leptospiral LPS, which is involved in adhesion and crawling, can induce the release of proinflammatory cytokines in infected cells (Tahara et al., 2018). We found that *L. interrogans* induces a ROCK-dependent cytoskeleton rearrangement and the formation of F-actin-lined vacuoles. Similar F-actin-lined vacuoles have been previously reported in disruption of the intestinal epithelial barrier by proinflammatory cytokines and in kidney epithelial cells that have lost cell polarity (Utech et al., 2005). Thus, the effect of the host immune response on AJC integrity and loss of cell polarity warrant further investigation. Apical-basolateral polarity in epithelial cells is regulated by intrinsic polarity proteins and signals from the adjacent cells, and a loss of polarity and microvilli disorganisation might be consequences of AJC disassembly (Pelaseyed & Bretscher, 2018). A previous study using a mouse model of infection showed that leptospiral kidney colonisation altered the organisation of the RPTEC brush border (Yamaguchi et al., 2018). Here, we found a transcriptional decrease in *myo7b*, which encodes a protein that links microvillar actin bundles to the cytoplasmic domain of cadherins for proper localisation of the intermicrovillar adhesion complex and for microvilli stability (Weck et al., 2016), suggesting that *L. interrogans* might disturb the microvilli structure. The direct binding of leptospiral proteins with host proteins also needs to be considered, since macromolecular interactions involving E-cad and microbial factors can lead to increase endocytosis (Dash, Duraivelan, & Samanta, 2021), potentiate GEFH1-dependent RhoA activation for TJ disruption (Huber, 2020) and perturb epithelial polarity (Tapia et al., 2017).

In conclusion, the use of an RPTEC/TERT1 cell infection model to study the pathogenic mechanisms of *L. interrogans* allowed us to mimic the paracellular route of leptospiral transmigration reported previously in *in vivo* studies and provided an opportunity to identify and analyse new players in leptospiral pathogenesis. Our results clearly show that *L. interrogans* induces AJC disassembly and furthers our understanding of the process of bacterial dissemination in the host. Mechanisms of AJC disassembly induced by enteropathogenic and enterohemorrhagic *Escherichia coli* include several integrated pathways, such as actin rearrangement, microtubule network disruption, vesicle traffic disruption and inhibition of the renewal of TJ proteins (Ugalde-Silva et al., 2016). In *L. interrogans*-infected RPTECs, E-cad endocytosis and ROCK-dependent cytoskeleton rearrangement induce AJC disassembly. The increase in cingulin in the soluble fraction suggested that cingulin failed to inhibit GEFH-1 at TJs, possibly inducing a RhoA/ROCK-dependent feed forward loop that further drives F-actin rearrangement. However, we could not rule out the role of other Rho regulatory proteins such as p120-catenin which is altered in *L. interrogans*-infected RPTECs (Schackmann, Tenhagen, van de Ven, & Derksen, 2013) (Figure 8). Moreover, the tight interactions of *L. interrogans* with the plasma membrane and efficient

propulsion of *L. interrogans* using back-and-forth movements can facilitate their invasion through AJCs and apply an additional mechanical force to enhance AJC disassembly (Abe, Kuribayashi, Takabe, & Nakamura, 2020).

## 4 | EXPERIMENTAL PROCEDURES

### 4.1 | Bacterial strains and culture conditions

*Leptospira interrogans* serovar Manilae strain UP-MMC-NIID (Koizumi & Watanabe, 2004) was propagated in 3-week-old specific pathogen-free C3H/HeJ mice to maintain the virulence. All animal experiments were performed in accordance with the guidelines for the care and use of laboratory animals of the University of the Ryukyus (Okinawa, Japan). Experimental protocols were approved by the Committee for Animal Experiments at the University of the Ryukyus (Permit Number: A2018071).

*Leptospira interrogans*, after no more than three passages, and *L. biflexa* serovar Patoc strain Patoc I strains were routinely cultured in Ellinghausen-McCullough-Johnson-Harris (EMJH) broth at 30°C stationary. *Leptospira interrogans* was diluted 20-fold and *L. biflexa* was diluted 40-fold in fresh EMJH and cultured for 3 days with shaking at 30°C for cell infection experiments.

### 4.2 | Cell culture

RPTEC/TERT1 (ATCC® CRL-4031™) cells were grown in Dulbecco's Modified Eagle Medium/Nutrient Mixture F-12 Ham (DMEM/F-12 Ham; Sigma-Aldrich) supplemented with 5 pM triiodothyronine, 10 ng/ml recombinant human epidermal growth factor, 3.5 µg/ml ascorbic acid, 5 µg/ml transferrin, 5 µg/ml insulin, 8.65 ng/ml sodium selenite and 100 µg/ml G418. The cells were seeded at a density of  $1.3 \times 10^6$  cells per well in polyethylene terephthalate hanging cell culture inserts, with a pore size of 1 µm (Millipore), in the upper chamber of a six-well plate or a chamber slide to measure the kinetics of bacterial attachment to the plasma membrane. Cells were maintained in a humidified incubator at 37°C and 5% CO<sub>2</sub> for 7–10 days after reaching confluence to allow monolayer maturation, and medium was exchanged every 2 days. The transepithelial electrical resistance (TEER) of the monolayers was measured using a Millicell-ERS cell resistance indicator (Millipore). After subtraction of the value of a cell-free filter (blank), the mean TEER value was expressed as Ωcm<sup>2</sup>. The TEER of cells before infection was designated as the baseline values. The percentage TEER relative to the baseline value was calculated using the following formula: (TEER of experimental wells/baseline TEER of experimental wells) × 100%.

### 4.3 | Cell infection

The cells were infected with leptospires at a multiplicity of infection (-MOI) of 100 from the basolateral side containing supplement-free

DMEM/F-12 Ham medium. In the experiments involving the use of inhibitors, they were added from 1 hr before infection (Figure 6, Figures S5–S8) or from 2 hr pi (Figure 7, Figure S9). The inhibitors used were 20  $\mu\text{M}$  Y27632 (Nacalai), 20  $\mu\text{M}$  H1152 (Adipogene), 60  $\mu\text{M}$  dynasore (Sigma-Aldrich), or 7.5  $\mu\text{M}$  Pitstop2 (Sigma-Aldrich). Cells were then incubated at 37°C and 5% CO<sub>2</sub> during infection and lysed for RNA, DNA or protein extraction or fixed for electron microscopy, immunostaining or cell death analysis.

To determine the relative number of gentamicin-protected and cell-associated bacteria, at 5 hr p.i. infected cells were transferred to a six-well plate containing pre-warmed DMEM/F-12 Ham medium containing gentamicin (40  $\mu\text{g ml}^{-1}$ ) or DMEM/F-12 Ham without antibiotic, respectively. Infected RPTECs were lysed with 300  $\mu\text{l}$  of distilled water at 6 hr or 24 hr p.i., and 100  $\mu\text{l}$  of each lysate were two-fold diluted with EMJH broth on 96-well plates. The plates were incubated at 30°C for 1 day or 2 days for *L. biflexa* and *L. interrogans*, respectively. The limiting dilution, which showed surviving leptospire, was determined by dark-field microscope (Nikaido et al., 2019).

#### 4.4 | Electron microscopy (SEM, TEM, and FIB-SEM tomography)

Infected RPTECs were pre-fixed at 6 and 24 hr p.i. with 2.5% glutaraldehyde in phosphate buffer (PB; 0.1 M, pH 7.4), and then were post-fixed with 1% osmium tetroxide in the same buffer. Specimens were stained overnight *en bloc* with a 2% (w/v) uranyl acetate aqueous solution and embedded in epoxy resin according to standard protocol.

For SEM of a wide-area, semi-thin sections (ca. 250 nm thickness) were stained with lead citrate solution (Reynolds, 1963) and observed under a scanning electron microscope (TM3030; Hitachi, Japan) using the backscattered electron mode, with accelerating voltage at 15 keV. SEM was carried out in the Research Laboratory Center at the University of the Ryukyus. Images shown were processed by inverting black/white.

Volume microscopy was performed using a focused ion beam scanning electron microscope (Helios 650; FEI Company, Eindhoven, The Netherlands). Milling was performed with a gallium ion beam at 30 kV and 770 pA, and the imaging was done at 1.5 keV, 800 pA, 6,144  $\times$  4,096 pixel frame size, 6  $\mu\text{s}$  dwell time, with 65 Å pixel size, and 200 Å section thickness (Kizilyaprak, Longo, Daraspe, & Humbel, 2015). After milling at 52°, the fresh surface was tilted to 90° and imaged normal to the electron beam (see accompanying video of Kizilyaprak et al., 2015). The images were aligned with IMOD using cross-correlation (Kremer, Mastronarde, & McIntosh, 1996).

For high resolution-TEM, ultra-thin sections (60 nm thick) were stained with lead citrate solution (Reynolds, 1963) and examined with a transmission electron microscope (Talos L120C; Thermo Fisher Scientific, Eindhoven, The Netherlands) at 120 keV acceleration voltage, and images were recorded using a Ceta 2 M16 4 k  $\times$  4 k camera (Thermo Fischer Scientific, Eindhoven, The Netherlands).

#### 4.5 | Adhesion-crawling assay

Swimming, adhering and crawling *Leptospira* cells were performed as previously described (Xu et al., 2020). Briefly, RPTECs were observed using a dark-field microscope (Eclipse-Ci; Nikon, Japan; Objective lens: Plan 20 $\times$ /0.40, Plan 40 $\times$ /0.65, Nikon; Condenser: Dark field Condenser Oil 1.43–1.20, Nikon) and recorded using a CMOS-camera (DMK23U021; Imaging Source, Taipei, Taiwan) at 30 frames per second. The fractions of adhering, crawling, or swimming cells were measured using an Image J software (NIH, MD, USA) and VBA macros in Microsoft Excel. Adhering or crawling cells were distinguished from swimming cells by a difference in the focus, and adhering cells were discriminated from crawling cells based on the criteria of both crawling speed (<1  $\mu\text{m/s}$ ) and the slope of the mean square displacement (MSD) versus time double-logarithmic plot (<0.5). The MSD slopes of diffusive crawling with lower net migration were  $\sim$ 1, as the directivity of crawling increased, the value got closer to 2 (Xu et al., 2020).

#### 4.6 | Quantitative real-time PCR

One millilitre of the apical culture supernatant or lysed infected RPTECs were used for DNA extraction as described previously (Toma & Suzuki, 2020). Two microliters of DNA and 0.5  $\mu\text{M}$  of both the forward and reverse primers for the *lipL32* gene in *L. interrogans* as described by Bourhy, Bremont, Zinini, Giry, and Picardeau (2011), and the 16S rRNA gene in *L. biflexa* as described by Thibeaux et al. (2018), were added to a mixture containing Brilliant III SYBR Green QPCR master mix (Stratagene, Agilent Technologies). The total number of bacteria was determined using a standard curve generated by the serial dilution of genomic DNA extracted from in vitro-cultivated bacteria as described previously (Toma et al., 2011).

#### 4.7 | RNA sequencing

RNA was isolated from infected RPTECs by using TRIzol and the RNeasy Mini kit (Qiagen) according to the manufacturer's instructions. Total RNA was quantified and qualified using the Agilent Tape Station 2,200 (Agilent Technologies). Sequencing libraries were generated using the NEBNext® Ultra™ FNA Library Prep Kit for Illumina® (NEB, USA). Libraries were sequenced on an Illumina HiSeq platform, and 125 bp/150 bp paired-end reads were generated. Prior to differential gene expression analysis, for each sequenced library, the read counts were adjusted by the edgeR program package through the scaling normalisation method. Differential expression analysis was performed using the DESeq R package (1.20.0). The *p* values were adjusted using the Benjamini and Hochberg method.

## 4.8 | Immunostaining

For the analysis of AJC proteins, RPTECs were fixed in cold-methanol for 15 min, permeabilized, and blocked with 5% bovine serum albumin (BSA) and 1% Triton X-100 in Tris-buffered saline (TBS; 50 mM Tris and 150 mM NaCl [pH 7.4]) for 15 min. For the dual immunostaining of bacteria and LAMP-1 and F-actin staining, infected cells were fixed with 2% paraformaldehyde in phosphate-buffered saline for 2 hr, at 4°C and washed twice with TBS. The membrane was detached from the hanging culture inserts before immunostaining.

Antibodies were diluted in TBS containing 1% BSA and 0.1% Triton X-100. The primary antibodies were a rabbit polyclonal anti-*L. interrogans* diluted (1:500 dilution; kindly provided by Sharon YAM Villanueva, University of the Philippines), anti-*L. biflexa* (1:500; Affinity BioReagents), anti-LAMP1 (1:200; sc-20,011, Santa Cruz), mouse monoclonal anti-E-cadherin (1:50; sc-8,426, Santa Cruz), mouse monoclonal anti-acetylated tubulin (1:100; T7451, Sigma-Aldrich), rabbit monoclonal anti-E-cadherin (1:50; #3195, Cell Signalling), mouse monoclonal anti-occludin (1:50; sc-133,256, Santa Cruz), rabbit polyclonal anti-claudin-10 (1:50; ab52234 Abcam), rabbit monoclonal anti-ZO-1 (1:200; #13663, Cell Signalling), mouse monoclonal anti-cingulin (1:50; sc-365,264, Santa Cruz), and mouse monoclonal anti-p120 catenin (1:50; sc-23,872, Santa Cruz). F-actin was stained with a 1:1,000 dilution of rhodamine phalloidin (Abcam). Cells were counterstained with a 1:100 dilution of TO-PRO™-3 (Invitrogen) to label the DNA. Secondary antibodies, purchased from Jackson ImmunoResearch, used for immunofluorescence analysis included anti-rabbit Alexa 488- (1:100; #711-545-152), Cy3- (1:100; #711-165-152) or Alexa 647-conjugated (1:100, #711-605-152); and anti-mouse Alexa 488- (1:100; #715-545-151) or Cy3-conjugated (1:100; #715-165-151). The compiled Z-stack images were acquired on a Leica TCS-SPE confocal laser-scanning microscope after mounting with SlowFade™ Diamond Antifade Mountant (Invitrogen) using LEICA LAS AF acquisition software (Leica Microsystems).

## 4.9 | Immunoblots

Infected cells were lysed with a mild lysis buffer (20 mM Tris-HCl, pH 7.4, 150 mM NaCl, 0.1% NP-40 supplemented with a protease inhibitor cocktail [Roche]) and cell lysates were collected with a cell scrapper for centrifugation. The supernatant was analysed as the soluble fraction, and the pellet was resuspended in TBS buffer and analysed as the insoluble fraction. Both fractions were mixed with Laemmli sample buffer (Laemmli, 1970) and heated for 10 min at 100°C. The insoluble fractions were sonicated for 3 min. Proteins in the supernatants of infected RPTECs (apical and basal sides) were precipitated with 10% trichloroacetic acid. The samples were separated by 7.5% or 10% sodium dodecyl sulphate-polyacrylamide gel electrophoresis and further processed for western blotting.

Primary antibodies used for western blotting included rabbit polyclonal anti-E-cadherin (1:2,000; sc-7,870, Santa Cruz), mouse monoclonal anti-occludin (1:100; sc-133,256, Santa Cruz), rabbit monoclonal

anti- $\beta$ -tubulin (1:2,500; #2128, Cell Signalling), mouse monoclonal anti-cingulin (1:100; sc-365,264, Santa Cruz), and a rabbit polyclonal anti- $\beta$ -actin (1:1,000; #4967, Cell Signalling). The secondary antibodies were a horseradish peroxidase (HRP)-anti-rabbit antibody (1:50,000; #111-035-144, Jackson ImmunoResearch), HRP-anti-mouse (1:10,000; #715-005-150, Jackson ImmunoResearch) and m-IgG $\kappa$  BP-HRP (1:1,000; sc-516,102, Santa Cruz). Bands were analysed using ImageJ software and protein levels normalised to a loading control.

## 4.10 | Cell death analysis

For the crystal violet assay, fixed cells were stained with 0.1% crystal violet solution. After extensive washing, the dye was eluted and analysed at 595 nm. The TUNEL assay was performed with the Dead-End fluorometric TUNEL system (Promega) as recommended by the manufacturer. Cisplatin (Wako) was used as a positive control.

## 4.11 | Statistical analysis

Statistical analysis was performed using the unpaired two-tailed Student's *t* tests. Differences were considered significant at  $p < .05$ .

## ACKNOWLEDGEMENTS

We gratefully acknowledge the generous support of the Okinawa Institute of Science and Technology, the Japanese Cabinet Office and the Research Laboratory Center at the University of the Ryukyus. We also acknowledge Sharon YAM Villanueva, University of the Philippines for providing anti-*L. interrogans* rabbit antisera and Takaki Motonaga for technical assistance. This work was supported by Japan Society for the Promotion of Science (JSPS) KAKENHI 18H02655 (Claudia Toma), 21H02732 (Claudia Toma), 18K07100 (SN), and 18J10834 (JX). [Correction added on May 25, 2021 after first online publication: "KAKENHI 18H02655" grant has been correctly attributed to Claudia Toma in this current version.]

## CONFLICT OF INTEREST

The authors declare no competing of financial interests.

## AUTHOR CONTRIBUTIONS

Isabel Sebastián, Nobuhiko Okura and Claudia Toma are involved in the conception or design of the study. Nobuhiko Okura, Bruno M. Humbel and Malgorzata Hall contributed with data acquisition and modelling of the electron microscopy experiments. Isabel Sebastián, Idam Hermawan, Chiaki Matsuura, Jun Xu, Shuichi Nakamura and Claudia Toma contributed with data acquisition and analysis of cell infection experiments. All authors contributed to the analysis or interpretation of data. Claudia Toma wrote the original draft of the manuscript. All authors contributed reviewing and editing the final version of the manuscript.

## DATA AVAILABILITY STATEMENT

The data that support the findings of this study are available from the corresponding author upon reasonable request.

## ORCID

Isabel Sebastián  <https://orcid.org/0000-0002-9265-6829>

Jun Xu  <https://orcid.org/0000-0002-1503-5623>

Idam Hermawan  <https://orcid.org/0000-0002-6813-9100>

Chiaki Matsuura  <https://orcid.org/0000-0002-0285-6772>

Shuichi Nakamura  <https://orcid.org/0000-0003-3972-7779>

Claudia Toma  <https://orcid.org/0000-0002-9852-1722>

## REFERENCES

- Abe, K., Kuribayashi, T., Takabe, K., & Nakamura, S. (2020). Implications of back-and-forth motion and powerful propulsion for spirochetal invasion. *Scientific Reports*, *10*, 13937.
- Aijaz, S., D'Atri, F., Citi, S., Balda, M. S., & Matter, K. (2005). Binding of GEF-H1 to the tight junction-associated adaptor cingulin results in inhibition of rho signaling and G1/S phase transition. *Developmental Cell*, *8*, 777–786.
- Aschauer, L., Gruber, L. N., Pfaller, W., Limonciel, A., Athersuch, T. J., Cavilli, R., ... Jennings, P. (2013). Delineation of the key aspects in the regulation of epithelial monolayer formation. *Molecular and Cellular Biology*, *33*, 2535–2550.
- Backert, S., Bernegger, S., Skórko-Glonek, J., & Wessler, S. (2018). Extracellular HtrA serine proteases: An emerging new strategy in bacterial pathogenesis. *Cellular Microbiology*, *20*, e12845.
- Barocchi, M. A., Ko, A. I., Reis, M. G., McDonald, K. L., & Riley, L. W. (2002). Rapid translocation of polarized MDCK cell monolayers by *Leptospira interrogans*, an invasive but nonintracellular pathogen. *Infection and Immunity*, *70*, 6926–6932.
- Bourhy, P., Bremont, S., Zinini, F., Giry, C., & Picardeau, M. (2011). Comparison of real-time PCR assays for detection of pathogenic *Leptospira* spp. in blood and identification of variations in target sequences. *Journal of Clinical Microbiology*, *49*, 2154–2160.
- Bryant, D. M., & Stow, J. L. (2004). The ins and outs of E-cadherin trafficking. *Trends in Cell Biology*, *14*, 427–434.
- Citi, S., Guerrero, D., Spadaro, D., & Shah, J. (2014). Epithelial junctions and rho family GTPases: The zonular signalosome. *Small GTPases*, *5*, 1–15.
- Citi, S., Paschoud, S., Pulimeno, P., Timolati, F., De Robertis, F., Jond, L., & Guillemot, L. (2009). The tight junction protein cingulin regulates gene expression and RhoA signaling. *Annals of the New York Academy of Sciences*, *1165*, 88–98.
- Citi, S., Pulimeno, P., & Paschoud, S. (2012). Cingulin, paracingulin, and PLEKHA7: Signaling and cytoskeletal adaptors at the apical junctional complex. *Annals of the New York Academy of Sciences*, *1257*, 125–132.
- Cruz, L. A., Vedula, P., Gutierrez, N., Shah, N., Rodriguez, S., Ayebe, B., ... Rodriguez, A. J. (2015). Balancing spatially regulated beta-Actin translation and dynamin-mediated endocytosis is required to assemble functional epithelial monolayers. *Cytoskeleton (Hoboken)*, *72*, 597–608.
- da Silva Tatley, F., Aldwell, F. E., Dunbier, A. K., & Guilford, P. J. (2003). N-terminal E-cadherin peptides act as decoy receptors for *Listeria monocytogenes*. *Infection and Immunity*, *71*, 1580–1583.
- Daroz, B. B., Fernandes, L. G. V., Teixeira, A. F., & Nascimento, A. L. T. O. (2020). In silico structural and functional characterization of HtrA proteins of *Leptospira* spp.: Possible implications in pathogenesis. *Tropical Medicine and Infectious Disease*, *28*, 179.
- Dash, S., Duraivelan, K., & Samanta, D. (2021). Cadherin-mediated host-pathogen interactions. *Cellular Microbiology*, *23*, e13316. <https://doi.org/10.1111/cmi.13316>
- De Brito, T., Menezes, L. F., Lima, D. M., Lourenco, S., Silva, A. M., & Alves, V. A. (2006). Immunohistochemical and in situ hybridization studies of the liver and kidney in human leptospirosis. *Virchows Archiv*, *448*, 576–583.
- De Brito, T., Silva, A. M. G. D., & Abreu, P. A. E. (2018). Pathology and pathogenesis of human leptospirosis: A commented review. *Revista do Instituto de Medicina Tropical de São Paulo*, *60*, e23.
- Devaux, C. A., Mezouar, S., & Mege, J. L. (2019). The E-cadherin cleavage associated to pathogenic bacteria infections can favor bacterial invasion and transmigration, Dysregulation of the immune response and cancer induction in humans. *Frontiers in Microbiology*, *10*, 2598.
- Drolia, R., & Bhunia, A. K. (2019). Crossing the intestinal barrier via listeria adhesion protein and Internalin A. *Trends in Microbiology*, *27*, 408–425.
- Eshghi, A., Gaultney, R. A., England, P., Brule, S., Miras, I., Sato, H., ... Picardeau, M. (2019). An extracellular *Leptospira interrogans* leucine-rich repeat protein binds human E- and VE-cadherins. *Cellular Microbiology*, *21*, e12949.
- Evangelista, K., Franco, R., Schwab, A., & Coburn, J. (2014). *Leptospira interrogans* binds to cadherins. *PLoS Neglected Tropical Diseases*, *8*, e2672.
- Forster, C. S., Johnson, K., Patel, V., Wax, R., Rodig, N., Barasch, J., ... Lee, R. S. (2017). Urinary NGAL deficiency in recurrent urinary tract infections. *Pediatric Nephrology*, *32*, 1077–1080.
- Grieve, A. G., & Rabouille, C. (2014). Extracellular cleavage of E-cadherin promotes epithelial cell extrusion. *Journal of Cell Science*, *127*, 3331–3346.
- Hoy, B., Lower, M., Weydig, C., Carra, G., Tegtmeyer, N., Geppert, T., ... Wessler, S. (2010). *Helicobacter pylori* HtrA is a new secreted virulence factor that cleaves E-cadherin to disrupt intercellular adhesion. *EMBO Reports*, *11*, 798–804.
- Hsu, S. H., Chu, C. H., Tian, Y. C., Chang, M. Y., Chou, L. F., Sun, Y. J., & Yang, C.-W. (2020). Crystal structure of *Leptospira* leucine-rich repeat 20 reveals a novel E-cadherin binding protein to induce NGAL expression in HK2 cells. *The Biochemical Journal*, *21*, 4313–4326.
- Huber, P. (2020). Targeting of the apical junctional complex by bacterial pathogens. *Biochimica et Biophysica Acta - Biomembranes*, *1862*, 183237.
- Ivanov, A. I., Parkos, C. A., & Nusrat, A. (2010). Cytoskeletal regulation of epithelial barrier function during inflammation. *The American Journal of Pathology*, *177*, 512–524.
- Kizilyaprak, C., Daraspe, J., & Humbel, B. M. (2014). Focused ion beam scanning electron microscopy in biology. *Journal of Microscopy*, *254*, 109–114.
- Kizilyaprak, C., Longo, G., Daraspe, J., & Humbel, B. M. (2015). Investigation of resins suitable for the preparation of biological sample for 3-D electron microscopy. *Journal of Structural Biology*, *189*, 135–146.
- Kizilyaprak, C., Stierhof, Y. D., & Humbel, B. M. (2019). Volume microscopy in biology: FIB-SEM tomography. *Tissue & Cell*, *57*, 123–128.
- Kochi, L. T., Fernandes, L. G. V., Souza, G. O., Vasconcellos, S. A., Heinemann, M. B., Romero, E. C., ... Nascimento, A. L. T. O. (2019). The interaction of two novel putative proteins of *Leptospira interrogans* with E-cadherin, plasminogen and complement components with potential role in bacterial infection. *Virulence*, *10*, 734–753.
- Koizumi, N., & Watanabe, H. (2004). Leptospiral immunoglobulin-like proteins elicit protective immunity. *Vaccine*, *22*, 1545–1552.
- Kourtidis, A., Ngok, S. P., & Anastasiadis, P. Z. (2013). p120 catenin: An essential regulator of cadherin stability, adhesion-induced signaling, and cancer progression. *Progress in Molecular Biology and Translational Science*, *116*, 409–432.
- Kowalczyk, A. P., & Nanes, B. A. (2012). Adherens junction turnover: Regulating adhesion through cadherin endocytosis, degradation, and recycling. *Sub-Cellular Biochemistry*, *60*, 197–222.
- Kremer, J. R., Mastronarde, D. N., & McIntosh, J. R. (1996). Computer visualization of three-dimensional image data using IMOD. *Journal of Structural Biology*, *116*, 71–76.
- Laemmli, U. K. (1970). Cleavage of structural proteins during the assembly of the head of bacteriophage T4. *Nature*, *227*, 680–685.

- Macia, E., Ehrlich, M., Massol, R., Boucrot, E., Brunner, C., & Kirchhausen, T. (2006). Dynasore, a cell-permeable inhibitor of dynamin. *Developmental Cell*, 10, 839–850.
- Marinho, M., Táparo, C. V., Oliveira-Júnior, I. S., Perri, S. H., & Cardoso, T. C. (2015). Tissue apoptosis in mice infected with *Leptospira interrogans* serovar Icterohaemorrhagiae. *Journal of Venomous Animals and Toxins Including Tropical Diseases*, 21, 22.
- Martens, E. C., Neumann, M., & Desai, M. S. (2018). Interactions of commensal and pathogenic microorganisms with the intestinal mucosal barrier. *Nature Reviews. Microbiology*, 16, 457–470.
- Martinez-Lopez, D. G., Fahey, M., & Coburn, J. (2010). Responses of human endothelial cells to pathogenic and non-pathogenic *Leptospira* species. *PLoS Neglected Tropical Diseases*, 4, e918.
- McCormack, J., Welsh, N. J., & Braga, V. M. M. (2013). Cycling around cell-cell adhesion with rho GTPase regulators. *Journal of Cell Science*, 126, 379–391.
- Miyahara, S., Saito, M., Kanemaru, T., Villanueva, S. Y., Gloriani, N. G., & Yoshida, S. (2014). Destruction of the hepatocyte junction by intercellular invasion of *Leptospira* causes jaundice in a hamster model of Weil's disease. *International Journal of Experimental Pathology*, 95, 271–281.
- Moreno-Torres, A., Malvido-Jimenez, I. R., de la Pena-Moctezuma, A., Castillo Sanchez, L. O., Fraga, T. R., Barbosa, A. S., ... Sahagún-Ruiz, A. (2019). Culture-attenuated pathogenic *Leptospira* lose the ability to survive to complement-mediated-killing due to lower expression of factor H binding proteins. *Microbes and Infection*, 21, 377–385.
- Nikaido, Y., Ogawa, M., Fukuda, K., Yokoyama, M., Kanemaru, T., Nakayama, T., & Saito, M. (2019). Transbronchial invasion and proliferation of *Leptospira interrogans* in lung without inflammatory cell infiltration in a hamster model. *Infection and Immunity*, 87, e00727–19.
- Pelaseyed, T., & Bretscher, A. (2018). Regulation of Actin-based apical structures on epithelial cells. *Journal of Cell Science*, 131, jcs221853.
- Pentecost, M., Kumaran, J., Ghosh, P., & Amieva, M. R. (2010). *Listeria monocytogenes* internalin B activates junctional endocytosis to accelerate intestinal invasion. *PLoS Pathogens*, 6, e1000900.
- Picardeau, M. (2017). Virulence of the zoonotic agent of leptospirosis: Still terra incognita? *Nature Reviews. Microbiology*, 15, 297–307.
- Preta, G., Cronin, J. G., & Sheldon, I. M. (2015). Dynasore – Not just a dynamin inhibitor. *Cell Communication and Signalling*, 13, 24.
- Ratet, G., Veyrier, F. J., Fanton d'Andon, M., Kammerscheit, X., Nicola, M. A., Picardeau, M., ... Werts, C. (2014). Live imaging of bioluminescent *Leptospira interrogans* in mice reveals renal colonization as a stealth escape from the blood defenses and antibiotics. *PLoS Neglected Tropical Diseases*, 8, e3359.
- Reynolds, E. S. (1963). The use of lead citrate at high pH as an electron-opaque stain in electron microscopy. *The Journal of Cell Biology*, 17, 208–212.
- Rusu, A. D., & Georgiou, M. (2020). The multifarious regulation of the apical junctional complex. *Open Biology*, 10, 190278.
- Sallustio, F., Constantino, V., Cox, S. N., Loverre, A., Divella, C., Rizzi, M., & Schena, F. P. (2013). Human renal stem/progenitor cells repair tubular epithelial cell injury through TLR2-driven inhibin-A and microvesicle-shuttled decorin. *Kidney International*, 83, 392–403.
- Samarin, S. N., Ivanov, A. I., Flatau, G., Parkos, C. A., & Nusrat, A. (2007). Rho/rho-associated kinase-II signaling mediates disassembly of epithelial apical junctions. *Molecular Biology of the Cell*, 18, 3429–3439.
- Sato, H., & Coburn, J. (2017). *Leptospira interrogans* causes quantitative and morphological disturbances in adherens junctions and other biological groups of proteins in human endothelial cells. *PLoS Neglected Tropical Diseases*, 11, e0005830.
- Satou, K., Shimoji, M., Tamotsu, H., Juan, A., Ashimine, N., Shinzato, M., ... Hirano, T. (2015). Complete genome sequences of low-passage virulent and high-passage Avirulent variants of pathogenic *Leptospira interrogans* Serovar Manilae strain UP-MMC-NIID, originally isolated from a patient with severe leptospirosis, determined using PacBio single-molecule real-time technology. *Genome Announcements*, 3, e00882-15.
- Schackmann, R. C., Tenhagen, M., van de Ven, R. A., & Derksen, P. W. (2013). p120-catenin in cancer – Mechanisms, models and opportunities for intervention. *Journal of Cell Science*, 126, 3515–3525.
- Schossleitner, K., Rauscher, S., Gröger, M., Friedl, H. P., Finsterwalder, R., Haberthuer, A., ... Petzelbauer, P. (2016). Evidence that Cingulin regulates endothelial barrier function in vitro and in vivo. *Arteriosclerosis, Thrombosis, and Vascular Biology*, 36, 647–654.
- Shrestha, S., Somji, S., Sens, D. A., Slusser-Nore, A., Patel, D. H., Savage, E., & Garrett, S. H. (2017). Human renal tubular cells contain CD24/CD133 progenitor cell populations: Implications for tubular regeneration after toxicant induced damage using cadmium as a model. *Toxicology and Applied Pharmacology*, 331, 116–129.
- Singh, A. P., Sharma, S., Pagarware, K., Siraji, R. A., Ansari, I., Mandal, A., ... Aijaz, S. (2018). Enteropathogenic *E. coli* effectors EspF and Map independently disrupt tight junctions through distinct mechanisms involving transcriptional and post-transcriptional regulation. *Scientific Reports*, 8, 3719.
- Tahara, H., Takabe, K., Sasaki, Y., Kasuga, K., Kawamot, O. A., Koizumi, N., & Nakamura, S. (2018). The mechanism of two-phase motility in the spirochete *Leptospira*: Swimming and crawling. *Science Advances*, 4, eaar7975.
- Tapia, R., Kralicek, S. E., & Hecht, G. A. (2017). Modulation of epithelial cell polarity by bacterial pathogens. *Annals of the New York Academy of Sciences*, 1405, 16–24.
- Thibeaux, R., Girault, D., Bierque, E., Soupe-Gilbert, M. E., Rettinger, A., Douyere, A., ... Goarant, C. (2018). Biodiversity of environmental *Leptospira*: Improving identification and revisiting the diagnosis. *Frontiers in Microbiology*, 9, 816.
- Tian, Y.-C., Chen, Y.-C., Hung, C.-C., Chang, C.-T., Wu, M.-S., Phillips, A. O., & Yang, C.-W. (2006). Leptospiral outer membrane protein induces extracellular matrix accumulation through a TGF- $\beta$ 1/Smad-dependent pathway. *Journal of the American Society of Nephrology*, 17, 2792–2798.
- Toma, C., Okura, N., Takayama, C., & Suzuki, T. (2011). Characteristic features of intracellular pathogenic *Leptospira* in infected murine macrophages. *Cellular Microbiology*, 13, 1783–1792.
- Toma, C., & Suzuki, T. (2020). Evaluation of intracellular trafficking in macrophages. *Methods in Molecular Biology*, 2134, 199–206.
- Tsukita, S., Tanaka, H., & Tamura, A. (2019). The Claudins: From tight junctions to biological systems. *Trends in Biochemical Sciences*, 44, 141–152.
- Ugalde-Silva, P., Gonzalez-Lugo, O., & Navarro-Garcia, F. (2016). Tight junction disruption induced by type 3 secretion system effectors injected by Enteropathogenic and Enterohemorrhagic *Escherichia coli*. *Frontiers in Cellular and Infection Microbiology*, 6, 87.
- Utech, M., Ivanov, A. I., Samarin, S. N., Bruewer, M., Turner, J. R., Mrsny, R. J., ... Nusrat, A. (2005). Mechanisms of IFN- $\gamma$ -induced endocytosis of tight junction proteins: Myosin II-dependent vacuolization of the apical plasma membrane. *Molecular Biology of the Cell*, 16, 5040–5052.
- van den Ingh, T. S. G. A. M., & Hartman, E. G. (1986). Pathology of acute *Leptospira interrogans* serotype icterohaemorrhagiae infection in the Syrian hamster. *Veterinary Microbiology*, 12, 367–376.
- van Roy, F., & Bex, G. (2008). The cell-cell adhesion molecule E-cadherin. *Cellular and Molecular Life Sciences*, 65, 3756–3788.
- Weck, M. L., Crawley, S. W., Stone, C. R., & Tyska, M. J. (2016). Myosin-7b promotes distal tip localization of the Intermicrovillar adhesion complex. *Current Biology*, 26, 2717–2728.
- Wieser, M., Stadler, G., Jennings, P., Streubel, B., Pfaller, W., Ambros, P., ... Grillari-Voglauer, R. (2008). hTERT alone immortalizes epithelial cells of renal proximal tubules without changing their functional characteristics. *American Journal of Physiology - Renal Physiology*, 295, F1365–F1375.



- Wunder, E. A., Figueira, C. P., Benaroudj, N., Hu, B., Tong, B. A., Trajtenberg, F., ... Ko, A. I. (2016). A novel flagellar sheath protein, FcpA, determines filament coiling, translational motility and virulence for the *Leptospira* spirochete. *Molecular Microbiology*, *101*, 457–470.
- Xu, J., Koizumi, N., & Nakamura, S. (2020). Crawling motility on the host tissue surfaces is associated with the pathogenicity of the zoonotic spirochete *Leptospira*. *Frontiers in Microbiology*, *11*, 1886.
- Yamaguchi, T., Higa, N., Okura, N., Matsumoto, A., Hermawan, I., Yamashiro, T., ... Toma, C. (2018). Characterizing interactions of *Leptospira interrogans* with proximal renal tubule epithelial cells. *BMC Microbiology*, *18*, 64.
- Zihni, C., Mills, C., Matter, K., & Balda, M. S. (2016). Tight junctions: From simple barriers to multifunctional molecular gates. *Nature Reviews. Molecular Cell Biology*, *17*, 564–580.

## SUPPORTING INFORMATION

Additional supporting information may be found online in the Supporting Information section at the end of this article.

**How to cite this article:** Sebastián, I., Okura, N., Humbel, B. M., Xu, J., Hermawan, I., Matsuura, C., Hall, M., Takayama, C., Yamashiro, T., Nakamura, S., & Toma, C. (2021). Disassembly of the apical junctional complex during the transmigration of *Leptospira interrogans* across polarized renal proximal tubule epithelial cells. *Cellular Microbiology*, *23*(9), e13343. <https://doi.org/10.1111/cmi.13343>